Journal of Power Sources 250 (2014) 58–67

Contents lists available at ScienceDirect

Journal of Power Sources

journal homepage: www.elsevier.com/locate/jpowsour

Review

Simulation tool based on a physics model and an electrical analogy for an alkaline electrolyser

Christian Henao, Kodjo Agbossou*, Mhamed Hammoudi, Yves Dubé, Alben Cardenas

Hydrogen Research Institute and the Département de Génie électrique et Génie informatique of the Université du Québec à Trois-Rivières, Trois-Rivières, QC G9A 5H7, Canada

HIGHLIGHTS

- Physical and electrical behavior of alkaline electrolyser is simulated.
- An electrical analogy is used to emulate the behavior of the alkaline electrolyser.
- The impact of the operating temperature and pressure has been evaluated.
- The effect of gas bubbles adhering on the electrodes has been analyzed.

ARTICLE INFO

Article history:
Received 23 April 2013
Received in revised form
2 October 2013
Accepted 19 October 2013
Available online 25 November 2013

Keywords:
Alkaline electrolyser
Physics modeling
Electrical analogy
Hybrid system

ABSTRACT

This paper presents an alkaline electrolyser simulation tool (AEST). This new approach is based on a physics model of an electrolytic cell and an electrical analogy of the physical effects taking place in the electrolyser. The physics model has been developed taking into account the electrodes' electrochemical properties, the thermodynamics of the reaction, and the electrical properties of the electrode plates, membrane and electrolyte. The electrical analogy is used to integrate the physics model into the electrical simulation systems. The AEST is able to describe the electrolyser's physical and electrical performance and estimates the operating current as function of the voltage, temperature, pressure and electrolyte concentration. The technical information on the Hydrogen Research Institute (HRI) electrolyser has been used to set up the AEST. The start-up phase of the electrolyser has been analyzed for various operating temperatures, pressures and voltages. The steady-state response of the electrolyser (at constant temperature, pressure and concentration of electrolyte) has been simulated as an element of a possible hybrid system. Simulations have been carried out using MATLAB/Simulink/SimPowerSystems®.
© 2013 Elsevier B.V. All rights reserved.

1. Introduction

Nowadays, renewable energy systems combined with hydrogen production are being considered as a promising source of clean energy, ahead of fossil-based sources. In hydrogen production based on water electrolysis, there are three principal types of electrolysers: alkaline electrolyte, proton exchange membranes and high temperature steam. Alkaline electrolysers are the most mature, best-known and most used technology for hydrogen production.

Alkaline electrolyser models can also be divided into two groups. The first group is known as the characteristic models and the second one as the electrical models. The majority of the characteristic models are based on the semi-experimental coefficients found by fitting the current–voltage (i–V) curves obtained from the experimental data. Some interesting work in this field has been reported by Vanhanen et al. and Ulleberg [1,2]. These models have been used to obtain the electrolyser's i–V curve and the rate of hydrogen production [3,4]. In this kind of model the operating voltage is the result of the current applied as input. Physics modeling has been used recently [5–7] for alkaline electrolysers. This physics approach is focused on modeling separately the effects taking place in an electrolysis cell.

Electrical models of electrolysers are used to integrate these into electrical simulation systems. These electrical representations have been proposed in different research publications [8–11]. However most of those propose a simple resistance plus voltage source as the electrical equivalent system. Other authors use transfer functions to

* Corresponding author. Tel.: +1 819 376 5011x3911.
E-mail address: kodjo.agbossou@uqtr.ca (K. Agbossou).

0378-7753/$ – see front matter © 2013 Elsevier B.V. All rights reserved.
http://dx.doi.org/10.1016/j.jpowsour.2013.10.086

simulate the electrolysers in power systems and to evaluate hydrogen production strategies, control systems [12,13] and grid frequency regulation. This modeling approach is only valid for electrolysers working at constant power in a hydrogen production plant.

This paper proposes an Alkaline Electrolyser Simulation Tool (AEST) based on a physics model with an electrical analogy in order to emulate the physical and electrical behavior of the alkaline electrolyser.

This paper specifically describes in detail the proposed physics model for one alkaline cell. The validation of the physics model using the Hydrogen Research Institute (HRI) electrolyser [3] and Phoebus electrolyser [2] is also presented. The electrolyser's electrical analogy based on the physics model is explained. Finally, the simulation results using the proposed simulation tool for electrolyser start-up phase and steady-state operation are also presented.

2. Physics model

2.1. Electrolytic cell model

The proposed physics model considers separately every physical phenomenon taking place in the electrolysis process in an alkaline electrolyser. In this approach, the electrical current (i), the electrolyser's temperature (T) and pressure (P), and the electrolyte's molar concentration (m) have been set as the model's main parameters. The i–V relation is then defined by (1).

$$V_{cell} = E_{th} + V_{act-c-\theta} + V_{act-a-\theta} + (R_c + R_a + R_{ele} + R_{mem}) \cdot i \quad (1)$$

where V_{cell} is the alkaline cell voltage, E_{th} is the required voltage to start the electrolysis reaction, $V_{act\text{-}c\text{-}\theta}$ and $V_{act\text{-}a\text{-}\theta}$ are the electrodes' (cathode and anode) activation overvoltages, R_c and R_a are the electrode's plate resistances, $R_{ele\text{-}\varepsilon}$ is the electrolyte's resistance, R_{mem} is the membrane's resistance, and i is the operating current.

2.1.1. Water electrolysis' theoretical voltage

The voltage $E_{th(T,P,m)}$ has been defined using Nerst's equation with a T, m and P dependence (2). The first term of the equation is a thermodynamic approximation of the Gibbs energy ($E_{rev(T,1)}$) – in this model the correlation proposed in Refs. [7,14] has been used. The second part of the equation includes the pressure and the electrolyte concentration impact on the voltage [7].

$$E_{th(T,P,m)} = E_{rev(T,1)} - \frac{RT}{nF}\left[(P - p_{H_2O})^{\frac{3}{2}}/p_{H_2O}/p^*_{H_2O}\right] \quad (2)$$

where $R = 8.315$ J K^{-1} mol^{-1} is the universal gas constant, $n = 2$ is the number of electrons transferred in the electrolysis reaction, and $F = 96{,}485$ C mol^{-1} is the Faraday constant. The partial pressure of pure water vapor is given by p^*_{H2O} as well as the electrolyte partial pressure (electrolyte having a molarity m) by p_{H2O} [7–14].

2.1.2. Electrochemical electrodes' activation overvoltage

Tafel's approximation has been used to estimate the overvoltage due to the electrochemical activation of the electrode [7], which is defined as follows:

$$V_{act-a} = b_a \log\left(\frac{J_a}{J_{0-a}}\right), \quad V_{act-c} = b_c \log\left(\frac{J_c}{J_{0-c}}\right) \quad (3)$$

The overvoltage on the cathode is defined as $V_{act\text{-}c}$ and the one on the anode as $V_{act\text{-}a}$. b_a and b_c are the Tafel slope for anode and cathode respectively, they can be computed by using (4). J is the current density of the electrodes [15] given by (5). $J_{0\text{-}a}$ and $J_{0\text{-}c}$ are the exchange current densities for anode and cathode. In the literature, they are generally expressed in mA cm^{-2}.

$$b = \frac{2.303RT}{nF\alpha} \quad (4)$$

where α is the transfer coefficient which can be defined for the anode and the cathode respectively as α_a and α_c.

$$J = \frac{i}{S_{eff}} \quad (5)$$

where S_{eff} is the effective electrode surface in cm^2, and is defined by (6) as a function of the fractional electrode coverage (θ) of the gas bubbles adhering on the electrodes [16]. In this paper, the same value of θ is applied for both electrodes. The value of θ can be calculated using the empirical correlation proposed in Ref. [7].

$$S_{eff} = S(1 - \theta) \quad (6)$$

where S is the nominal electrode surface in cm^2.

The kinetic electrode parameters α_a, α_c, $J_{0\text{-}a}$ and $J_{0\text{-}c}$, have a value-dependence determined by the material choice of the catalyst, the operating temperature and the electrolyte type and weight–weight percentage (wt.%). In the HRI's alkaline electrolyser (described in Table 1), Nickel (Ni) at 99.99% of purity has been used as the catalyst for the cathode and anode as well as aqueous potassium hydroxide (KOH) at 30 wt.% (optimal weight–weight percentage for KOH electrolyte [7]). The approximations of $J_{0\text{-}c}$ and $J_{0\text{-}a}$ for the HRI electrolyser (data reported in Refs. [17–20]) can be modeled by (7) and (8), respectively.

$$J_{0-c} = 13.72491 - 0.09055T + 0.09055T^2 \quad (7)$$

$$J_{0-a} = 30.4 - 0.206T + 0.00035T^2 \quad (8)$$

The expressions describing the evolution of α_c and α_a have been found using experimental data published in Refs. [17–20] for the

Table 1
HRI's Electrolyser parameters.

Operating information		Description
Max. operating voltage		48–56 V
Operating pressure (P)		1 bar
Operating temperature (T)		0–353.15 K
Hydrogen production rate		1 Nm^3 h^{-1} at 80 °C
Electrical power reference		5 kW at 60 °C
Electrolyser's component		**Material**
Membrane		Zirfon
Anode		Nickel 99.99%
Cathode		Nickel 99.99%
Electrolyte		KOH at 30 wt. %
Symbol	**Description**	**Value**
n_{cell}	Number of electrolytic cells	24
d_{ac}	Anode–cathode gap	2.5 mm
d_{am}	Anode–membrane gap	1.25 mm
d_{cm}	Cathode–membrane gap	1.25 mm
S_m	Membrane surface area	0.03 m^2
e_m	Membrane thickness	0.5 mm
S_a, S_c	Anode and cathode surface area	0.03 m^2
e_a, e_c	Anode and cathode thickness	2 mm
L_a, L_c	Anode and cathode height	45 cm
$J_{0\text{-}c}$	Cathode exchange current density	(7)
$J_{0\text{-}a}$	Anode exchange current density	(8)
α_c	Cathode transfer coefficient	(9)
α_a	Anode transfer coefficient	(10)

given catalyst materials and electrolyte; the correlations used for the HRI electrolyser are given by (9) and (10) [7].

$$\alpha_c = 0.1175 + 0.00095 \cdot T \tag{9}$$

$$\alpha_a = 0.0675 + 0.00095 \cdot T \tag{10}$$

The bubble effect on the electrode surfaces is included in the electrode activation overvoltage definition.

The activation overvoltage of the electrodes taking into account θ is given by (11).

$$V_{act-\theta} = b\log\left(\frac{\frac{i}{S(1-\theta)}}{J_0}\right) \tag{11}$$

The activation overvoltage of the electrodes can be separated into two different parts as shown in (12).

$$V_{act-\theta} = V_{act} + V_\theta = b\log\left(\frac{J}{J_0}\right) + b\log(1-\theta) \tag{12}$$

where the first part (V_{act}) is related to the overvoltage as the result of the activation of the electrodes, and the second part (V_θ) represents the bubble overvoltage due to the coverage of electrode surface.

2.1.3. Electrical resistive phenomenon

Each component in the electrolytic cells is modeled as an electrical resistance. Then, R_a and R_c are the anode and the cathode resistances; R_{KOH} is the resistance of the electrolyte (in this case KOH), which is estimated by correlations taking into account temperature and concentration; R_{mem} is the resistance of the membrane separator. A bubble phenomenon affecting KOH resistivity is included in this approach.

2.1.3.1. Electrodes. The electrical conductivity of the Ni (σ_{Ni}), in S cm^{-1}, is defined by (13) as a function of T.

$$\sigma_{Ni} = 6000000 - 279650T + 532T^2 - 0.38057T^3 \tag{13}$$

The resistances of the electrodes, R_a and R_c, as a function of their geometry and conductivity are given by (14).

$$R_a = \frac{1}{\sigma_{Ni}}\left(\frac{L_a}{S_a}\right), \quad R_c = \frac{1}{\sigma_{Ni}}\left(\frac{L_c}{S_c}\right) \tag{14}$$

where S_a and S_c are respectively the anode and cathode cross-sections. L_a and L_c are the electrode thicknesses.

2.1.3.2. Electrolyte. The ionic conductivity of the KOH ($\sigma_{KOH\text{-}free}$) in S cm^{-1} depends on the temperature and the molar concentration (given by the m in mol m^{-3}) of the electrolyte. Empirical characterizations have been reported in Refs. [21,22]. The correlation published by Gilliam et al. [21] has been used in this work. This correlation is shown by (15).

$$\sigma_{KOH-free} = -2.04m - 0.0028m^2 + 0.005332mT + 207.2\frac{m}{T} + 0.001043m^3 - 0.0000003m^2T^2 \tag{15}$$

The gas bubbles created on the electrodes' surfaces go into the bulk electrolyte affecting the $\sigma_{KOH\text{-}free}$. This effect can be modeled by using the Bruggman equation (16) reported in [23].

$$\frac{\sigma_{KOH-e}}{\sigma_{KOH-free}} = (1-\varepsilon)^{\frac{3}{2}} \tag{16}$$

where $\sigma_{KOH\text{-}\varepsilon}$ is the new ionic conductivity of the electrolyte as the result of the bubbles presence in the bulk electrolyte. The relationship between ε and θ under specific conditions as reported in Ref. [24] is given by (17).

$$\varepsilon = \frac{2}{3}\theta \tag{17}$$

R_{ele} is defined as the sum of the bubble-free electrolyte's resistance ($R_{ele\text{-}free}$) and the resistance due to bubbles in the electrolyte ($R_{ele\text{-}\varepsilon}$), (18).

$$R_{ele} = R_{ele-free} + R_{ele-e} \tag{18}$$

The electrical resistance formula is also applied to calculate the resistance due to the electrolyte ($R_{ele\text{-}free}$), as shown in (19).

$$R_{ele-free} = \frac{1}{\sigma_{KOH-free}}\left(\frac{d_{am}}{S_a} + \frac{d_{cm}}{S_c}\right) \tag{19}$$

where d_{am} and d_{cm} are the distances between the electrodes (anode and cathode, respectively) and the membranes.

Finally the definition of $R_{ele\text{-}\varepsilon}$ is given by (20).

$$R_{ele-\varepsilon} = R_{ele-free}\left(\frac{1}{(1-\varepsilon)^{3/2}} - 1\right) \tag{20}$$

The existence of $R_{ele\text{-}\varepsilon}$ depends on the presence of a current passing through the alkaline cells and is calculated using $R_{ele\text{-}free}$ and ε as shown in (20). If the operating current is equal to zero, the $R_{ele\text{-}\varepsilon}$ is equal to zero too.

2.1.4. Membrane

The HRI electrolyser uses a non-organic membrane based on Zirfon. An empirical relation between electrical resistance and temperature for a 0.5 mm thickness Zirfon membrane has been reported in Ref. [25] in the form of (21), where S_m is the membrane surface in cm^2.

$$R_{mem} = \frac{0.060 + 80e^{T/50}}{10000S_m} \tag{21}$$

2.2. Physics model validation

The physics model has been developed based on a "*mean*" model. This model simulates only one electrolytic cell, and supposes that all the cells contained in the electrolyser (n_{cell}) have the same physical performance and behavior. The relationship between V_{cell} and the electrolyser's operating voltage V_{ele} is thus given by (22).

$$V_{ele} = n_{cell}V_{cell} \tag{22}$$

In this physics model, all the information needed to set up the electrolyser cell model is divided into two parts: the first part is devoted to the operating parameters, and the second part contains all the information relative to the electrode material, membrane, electrolyte concentration and cell geometry.

An atmospheric electrolyser has been used to make a first validation of the physics model. Table 1 presents a general description of the HRI's alkaline electrolyser used in this validation.

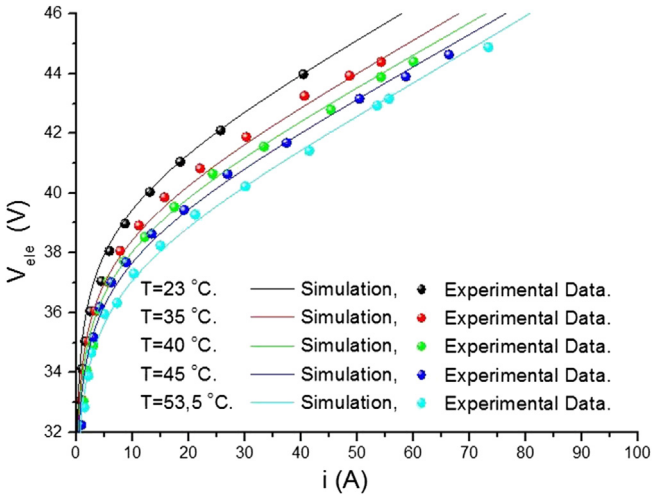

Fig. 1. Electrolyser's model validation at different temperatures for the HRI's electrolyser at atmospheric pressure.

Fig. 1 presents the comparison between the experimental and the simulation data of i–V curves at different temperatures for the HRI electrolyser.

Experimental data measured at HRI have been used to validate the proposed physics model. The i–V_{ele} simulation results shown in Fig. 1 for different operational temperatures have been calculated with the equations presented so far.

For purposes of comparison to our earlier work [3], Fig. 2 shows the same experimental data as in Fig. 1 but fitted with the parameters of that older model.

The results using the physics model are in better agreement with the experimental data than those using the model proposed in Ref. [3]. The accuracy of the new results is better irrespective of the operating temperature. The physics model is able to describe the i–V_{ele} response of the HRI electrolyser from the start-up period (low current) to maximal operating current at different temperatures, which means that it is an improvement of the way of modeling alkaline electrolysers operating at atmospheric pressure.

The aim of this comparison is to demonstrate the versatile character of the model proposed in this paper and its ability to be used to simulate the behavior of electrolysers even at different operating temperatures.

Table 2
Phoebus's Electrolyser parameters.

Operating information		Description
Max. operating voltage		30–40 V
Operating pressure (P)		7 bar
Operating temperature (T)		0–353.15 K
Electrical power		5 kW–26 kW
Electrolyser's component	**Material**	
Membrane	NiO diaphragms	
Anode	Ni/Co_3O_4/Fe on performed Ni-plate	
Cathode	C–Pt on performed Ni-plate	
Electrolyte	KOH at 30 wt.%	
Symbol	**Description**	**Value**
n_{cell}	Number of electrolytic cells	21
d_{ac}	Anode–cathode gap	Zero gap
d_{am}	Anode–membrane gap	Zero gap
d_{cm}	Cathode–membrane gap	Zero gap
S_m	Membrane surface area	0.25 m^2

The electrolyser model presented by Ulleberg in Ref. [2] has been used widely in the literature to simulate electrolysers in any kind of simulation systems. That model is based on a semi-empirical approach and is however restricted to a specific alkaline electrolyser. The Phoebus electrolyser [2] has been used to validate the model proposed by Ulleberg. A second validation for our physics model has thus been done using the Phoebus electrolyser. Table 2 presents a general description of that alkaline electrolyser.

The interest of simulating the Phoebus electrolyser using the physics model proposed in this paper is to show the response of the physics approach using a pressurized electrolyser and a zero gap technology in comparison to the results with the model proposed in Ref. [2].

Simulations for the Phoebus electrolyser have been carried out using physics model. Fig. 3 presents the simulation data with the experimental data reported in Ref. [2] for this electrolyser.

The simulated results in Fig. 3 show a good correlation with the experimental data. Thus, three operating temperatures for this electrolyser have been chosen in order to compare the results for

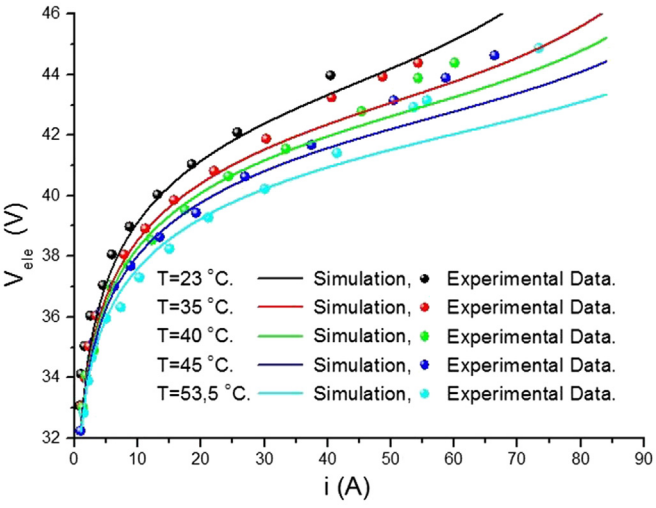

Fig. 2. Experimental data compared with the model propose in Ref. [3] for the HRI's electrolyser at atmospheric pressure.

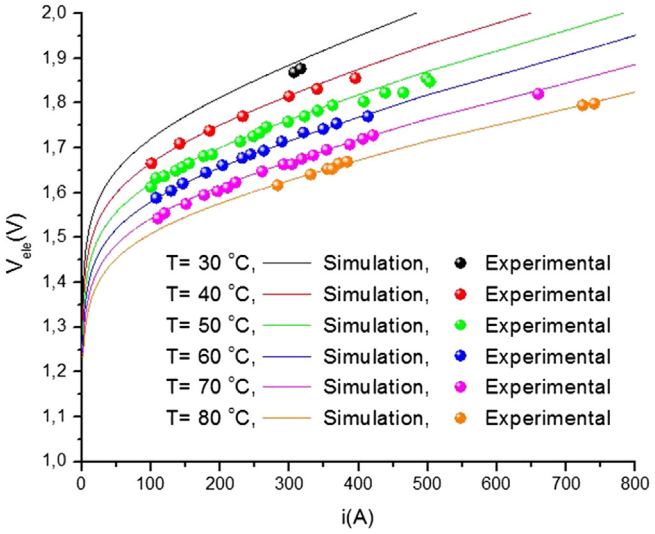

Fig. 3. Electrolyser's model validation at different temperatures for the Phoebus electrolyser at 7 bar.

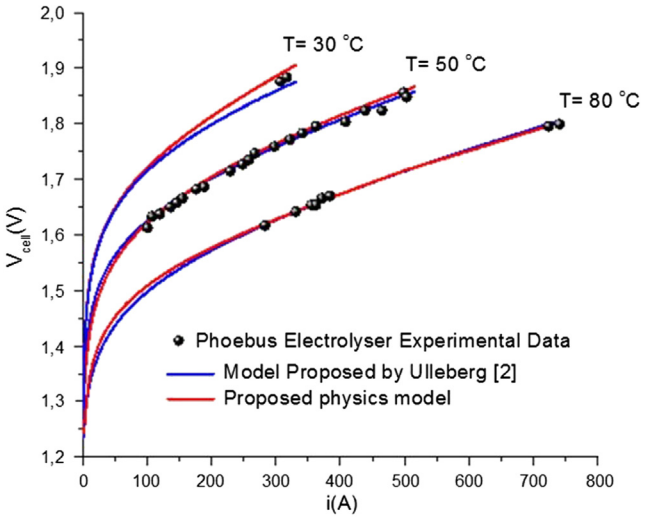

Fig. 4. Comparison between Ulleberg approach [2] and HRI's model for Phoebus electrolyser. V_{cell} for different temperatures at 7 bar.

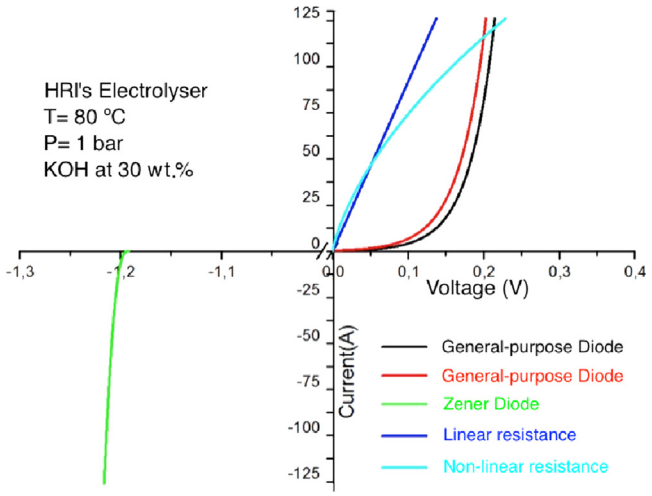

Fig. 5. Electrical behavior representation of the electrolyser's physics phenomenon.

the Phoebus electrolyser using physics model, Ulleberg's model [2] and experimental data. Fig. 4 presents the comparison at 30 °C, 50 °C and 80 °C.

As shown in Fig. 4, the Ulleberg approach and the physics model are equally good to emulate the electrical response of the Phoebus electrolyser. The evolution of these polarization curves for all three temperatures are in a good agreement with the experimental data. The difference between the two models lies in the fact that the physics model permits tracking the evolution of the pressure P and the molar concentration m with changing temperatures while Ulleberg's model considers these constant. Since in real electrolysers P and m (and maybe other "configuration parameters" as well) change with T, it follows that our physics model should be the better model to predict the behavior of such electrolytes.

To obtain an even more realistic simulation performance from the physics model, modules involving external thermal and pressure calculations could be added. In this way, and applied to hydrogen production, the efficiency calculations will be even more exact.

3. Electrolyser's electrical analogy and integration with power electronics

Power electronics interfaces are used to regulate the power transfer between energy sources and storage media to the electrolyser [9,26]. An electrolyser's electrical analogy has been developed in order to create an electrically programmed interface between the power electronics systems and the physics model. This interface permits to couple the physics model to the electrical simulation systems. This electrical analogy of electrolyser can be useful for many power control system based on hydrogen production.

3.1. Electrical analogy

The V–i relationship of the physical effects presented and modeled in Section 2 of this work, have been analyzed in order to establish similarities with the electrical behavior of some electronic components. One simulation has been carried out at 80 °C and 1 bar using the HRI electrolyser, and the results are shown in Fig. 5. These five electronic components, programmed using MATLAB/Simulink/SimPowerSystems®, are used to generate a circuit representing the electrical performance of the electrolyte (see Fig. 6).

3.1.1. Zener diode

The V–i characteristic of a Zener diode in reverse bias has some similarities to the voltage required by the electrochemical reaction of the electrolysis. The Zener diode voltage (BV) equivalent is described by (23).

$$\mathrm{BV} = -\left(E_{\mathrm{th}(T,P,m)} + V_{\theta-\mathrm{a}} + V_{\theta-\mathrm{c}}\right) \tag{23}$$

where E_{th} is the onset breakdown voltage; $V_{\theta\text{-a}}$ and $V_{\theta\text{-c}}$ are the non-linear terms simulating the overvoltage due to the gas bubbles adhering to the gas-evolving electrodes. This required breakdown voltage has to be reached before current starts to flow through the cells to initiate the electrolysis.

3.1.2. Rectifier diodes

The activation overvoltage of electrodes is similar to the forward voltage effect of a general-purpose (rectifier) diode in forward bias. The forward voltage has the same electrical behavior as the activation of the electrodes in an alkaline cell. The forward voltage is given by (24) for the cathode-diode and by (25) for the anode-diode analogy.

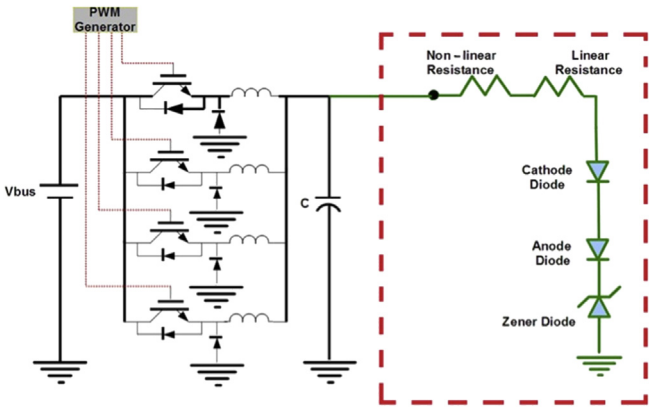

Fig. 6. The electrical electrolyser's analogy coupled to a multiphase buck converter.

$$V_{\text{diode-c}} = V_{\text{act-c}} \tag{24}$$

$$V_{\text{diode-a}} = V_{\text{act-a}} \tag{25}$$

3.1.3. Resistances

Linear resistive physical effects, which are part of the electrolyser, are grouped into a single resistor (R_Ω) as shown in (26). R_Ω has a linear behavior and its value depends only on T, the geometrical parameters, and the materials used to build the electrolytic cells.

$$R_\Omega = R_c + R_a + R_{\text{mem}} + R_{\text{ele-free}} \tag{26}$$

The $R_{\text{ele-}\varepsilon}$ is used as the non-linear resistor component in the electrolyser's electrical analogy.

3.2. Integration: DC/DC converter and electrolyser's electrical analogy

The electrolyser's cells require DC for operating; in this work a DC bus supplies this energy. In order to analyze and integrate the electrolyser model, a DC/DC power electronics converter has been used as power interface between DC bus and electrolyser, which allows the control of the power transfer from the DC source to the electrolyser by means of an adjustable duty cycle (α). In this work, a multiphase buck converter developed by IRH has been programmed using MATLAB/Simulink/SimPowerSystems® for the analysis of the transient response (see Section 4.1), and an ideal buck converter for the steady-state analysis (see Section 4.2). The electrical analogy of the electrolyser connected directly to the buck converter is shown in Fig. 6.

The initial state of the electrolyser is defined by R_Ω and the first term of BV (simple resistance in series with a Zener diode). If the value of V_c (voltage of the output capacitor of the buck converter) at the start is lower than BV, the current value is $i = 0$. Once V_c has exceeded BV a current i appears, therefore, i is calculated using (27).

$$i = \frac{V_C - \text{BV}}{R_\Omega} \tag{27}$$

The i is measured and used by the electrolyser's model to calculate all the new values (voltage and resistance, as shown in Fig. 7) of the electrical components of the electrolyser's electrical analogy.

In order to activate the electrodes, the current density J must be greater than the values $J_{0\text{-a}}$ and $J_{0\text{-c}}$ respectively for each electrode. The activation of the cathode is achieved only when $J > J_{0\text{-c}}$. When this current density condition is reached the first diode is added to the circuit. Therefore, current is defined by (28).

$$i = \frac{V_C - \text{BV} - V_{\text{diode-c}}}{R_\Omega} \tag{28}$$

The activation of the anode is determined by $J > J_{0\text{-a}}$. Once the current density satisfies this condition, the anode diode is activated, and hydrogen and oxygen can begin to be produced. The current then becomes (29).

$$i = \frac{V_C - \text{BV} - V_{\text{diode-c}} - V_{\text{diode-a}}}{R_\Omega} \tag{29}$$

Gas production within the cells causes bubbles to form on the electrodes. Some of these bubbles remain adhered to the electrodes while others will/can form a bubble curtain in the cross-section of the electrolyte. This gas production modifies the current somewhat. Then i can be redefined by (30).

$$i = \frac{V_C - \text{BV} - V_{\text{diode-c}} - V_{\text{diode-a}}}{R_\Omega + R_{\text{ele-}\varepsilon}} \tag{30}$$

The Alkaline Electrolyser Simulation Tool (AEST) is composed by the electrolyser's electrical analogy and the physics model as shown in Fig. 7. In AEST the i value is recalculated at every simulation step through the internal feedback calculation loop (i_{measured} – see Fig. 7). This loop measures the current flowing through the AEST and controlled by the DC/DC converter; this is used to estimate the new values (voltage and resistance) of the electrolyser's electrical analogy from the physics model. The i loop guarantees a good calculation of the electrolyser's operation parameters and a correct information feed-back in the coupling interface.

It should be noted that this electrolyser's current loop has been used in Ref. [8] to control an electrolyser in a wind-H2 hybrid network. The model used in Ref. [8] to emulate the electrolyser is a simplification of the model proposed in Ref. [2]. This simplification is based on a constant voltage source and constant resistance. These elements were used to perform the electrical analysis of the electrolyser current calculation. In this paper, the AEST is a more realistic module for the electrolyser emulation; the AEST is able to perform in electrical models. The proposed AEST has been integrated into an electrical simulation system using an electrical analogy with a closed current loop calculation implemented in order to estimate the current of the electrolyser.

The next section of this paper will show how the AEST could be used to analyze the start-up phase of an electrolyser using power electronics interface to control electrical power, this kind of simulations cannot be done using a constant model of the electrolyser.

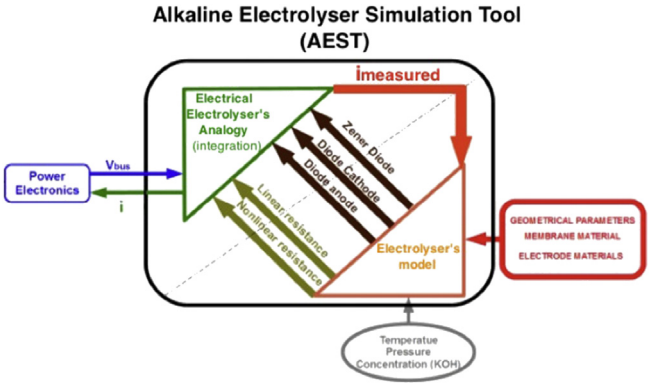

Fig. 7. The Electrical electrolyser's analogy coupled to the physics model.

4. Simulations results

The simulations have been carried out using the AEST and the buck converter (as shown in Fig. 6). The first group of simulations have been done in order to evaluate the starting up phase of the electrolyser and the influence of the changing of V, T, and P on the electrolyser's performance. These simulations have confirmed the influence of the operating parameters on the power consumption and on the operating current of the electrolyser. The start-up period of the electrolyser is also reported in this section. In the second group of simulations, the ideal DC/DC converter-AEST has been used in a hypothetical electrical hybrid (renewable source and diesel generator) topology with a hydrogen production system in order to observe the steady-state response of the system.

Table 3
Multiphase buck converter's electrical simulation parameters.

Symbol	Description	Value
L_1, L_2, L_3 and L_4	Inductance	0.3 mH
C	Capacitor	100 μF
V_{bus}	DC bus nominal voltage	48 V
Freq	IGBT commutation Frequency	15 kHz
N	Number of cells	4

4.1. Electrolyser's transient response

All simulations presented here have been made using the HRI electrolyser configuration with the multiphase buck converter (described in Table 3) used in Fig. 6. Different values of α have been applied in order to obtain different input voltages. The current generated by the imposition of a voltage αV_{bus} is also shown in Fig. 8.

The impact of temperature on the electrical performance of the simulation module has also been evaluated. Several simulations have been made in order to evaluate the electrical response of the system at different operating temperatures and pressures. The electrolyser current–voltage curve for one cell at different temperatures is shown in Fig. 9.

These results confirm that the temperature influences positively the electrolyser's current at a given operating voltage. The power absorbed by the electrolyser at a constant temperature of 80 °C and different operating pressures is shown in Fig. 10. When the operating pressure is increased, the current drawn by the electrolyser is reduced significantly.

4.2. Electrolyser's steady-state response

The AEST and the ideal DC/DC converter have been integrated into a possible hybrid hydrogen production system based on renewable energy in order to evaluate its steady-state response. The topology of the theoretical system is presented in Fig. 11.

This small stand-alone hybrid system includes a Wind-turbine generator (WT) and a Diesel generator (DG) as the power sources; where the DG is the backbone element of the system. This hybrid system represents the typical case in stand-alone areas, where hydrogen production can be used to reduce dependency on fossil fuels. The AC/DC converter is supposed to be an ideal converter. The electrolyser is integrated into the system as a power regulator component as well as a slave dump load. Electrolysers have recently been proposed to accomplish this challenge in small grids [27–30], using the surplus energy to produce hydrogen. Load power and wind speed are emulated using predefined profiles.

The power generated by the HRI's wind turbine (Bergey Excel 10 kW) is determined by using the correlation from experimental data (output power as a function of wind speed), as presented in Fig. 12.

A 12 kW DG has been used in these simulations; in order to improve the DG's efficiency, the DG's operation low power limit has been set at 5 kW. The operating conditions for the DG are defined by (31). The DG's power demand is determined by (32).

$$5\ \text{kW} \leq P_{\text{diesel}} \leq 12\ \text{kW} \tag{31}$$

$$P_{\text{diesel}} = P_{\text{wind}} - P_{\text{load}} \tag{32}$$

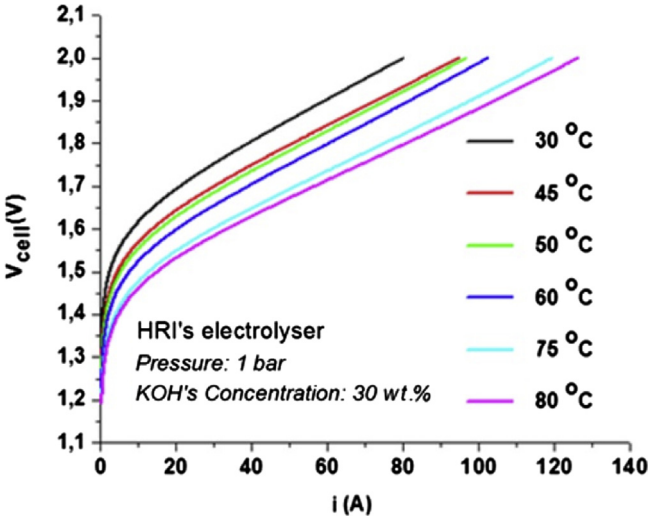

Fig. 9. Electrolyser's i–V curves at different operating temperatures.

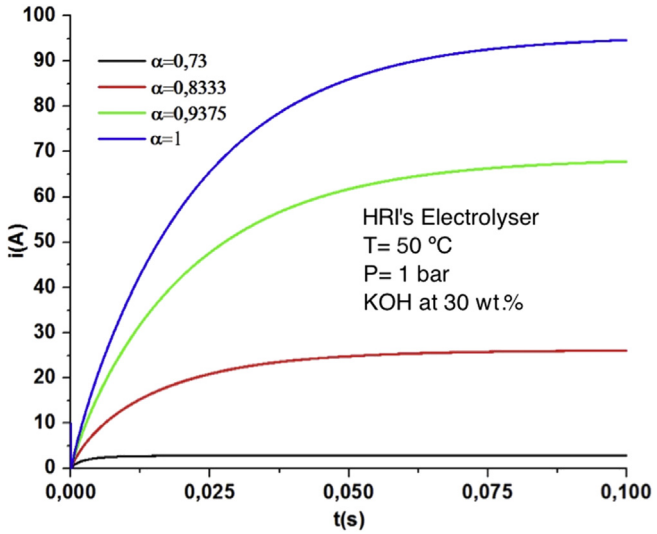

Fig. 8. Electrolyser's current response for different α values.

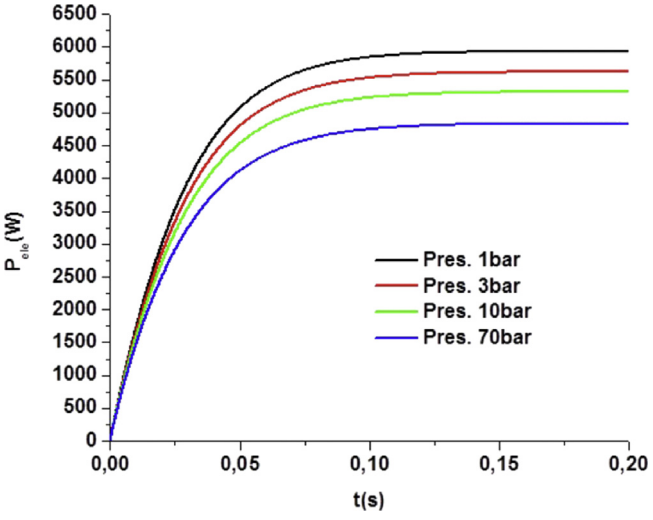

Fig. 10. Electrical power absorbed by the electrolyser at different operating pressures and at 80 °C.

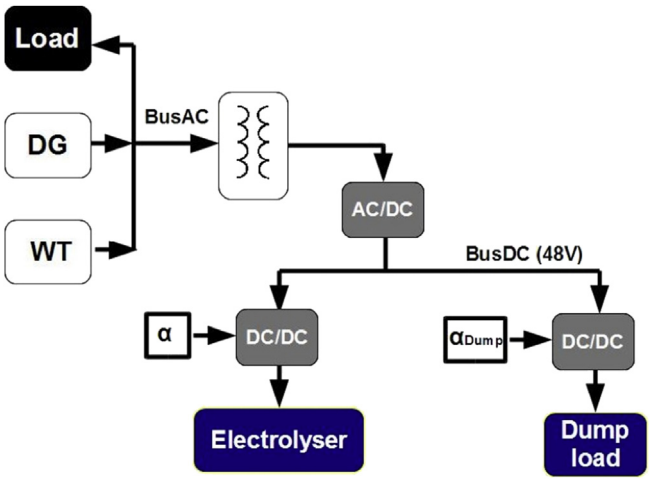

Fig. 11. Topology of hybrid hydrogen production system based on renewables.

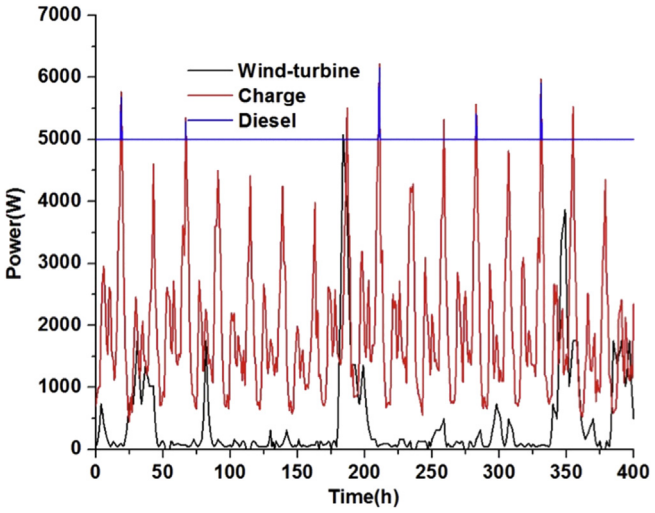

Fig. 13. WT, DG and charge power for 400 h.

Steady-state simulations have been carried out in MATLAB/Simulink® using a time scale of 1 s (simulation) equal to 1 h of wind profile. The power produced by the WT and the DG, as well as the power demanded by the load for 400 h of system operation are shown in Fig. 13. Under these conditions the DG supplies power constantly, albeit mostly at its low cutoff value of 5 kW, and higher only occasionally when the load power peaks and exceeds what the WT can produce at that moment. It is of course the excess power generated by the WT which gets channeled to the hydrogen-generating electrolyser (or elsewhere, as symbolized by the "dump load" in Fig. 11).

The available power is determined by (33) and shown in Fig. 14.

$$P_{\text{available}} = P_{\text{diesel}} + P_{\text{wind}} - P_{\text{load}} \tag{33}$$

This amount of electrical power must be absorbed by a regulator in order to avoid frequency grid perturbations [12].

The electrolyser is used as the master element to absorb the power excess of the system. However, P_{ele} is limited by T, P and m. Hence, a dump load is used as a second regulation component in slave mode; this dump load should absorb the amount of power, which the electrolyser is not able to use to produce hydrogen. The electrolyser and dump load powers must be equal to the available power as shown in (34).

$$P_{\text{available}} = P_{\text{dump}} + P_{\text{ele}} \tag{34}$$

P_{ele} is calculated using the coupling-system and taking into consideration the duty cycle α, the DC bus voltage and the electrolyser current ($P_{\text{ele}} = \alpha \cdot V_{\text{bus}} \cdot i$). i is estimated by using (30); this means that the electrolyser power in its steady-state can be given by (35).

$$P_{\text{ele}} = \alpha V_{\text{bus}} \left(\frac{\alpha V_{\text{bus}} - \text{BV} - V_{\text{diode-c}} - V_{\text{diode-a}}}{R_{\Omega} + R_{\text{ele}-\varepsilon}} \right) \tag{35}$$

$P_{\text{ele-max}}$ is found when $V_{\text{bus}} \approx V_{\text{c}}$ and $P_{\text{ele-min}}$ is fixed at 300 W. The electrolyser operates in these simulations at constant T, P and m, control is effected using different values of α as per the following conditions.

Case 1. : If $P_{\text{available}} < P_{\text{ele-min}}$, the electrolyser is turned off.

Case 2. : If $P_{\text{ele-min}} < P_{\text{ele}} < P_{\text{ele-max}}$, the electrolyser is turned on and the duty cycle used to control the buck converter is computed using (36).

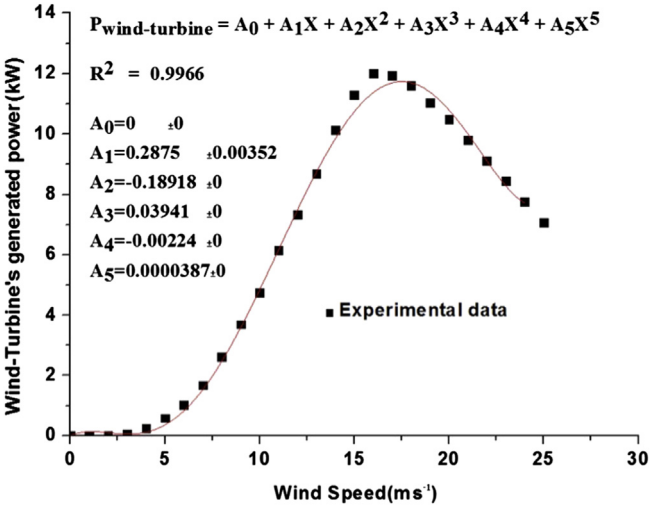

Fig. 12. WT characteristic curve.

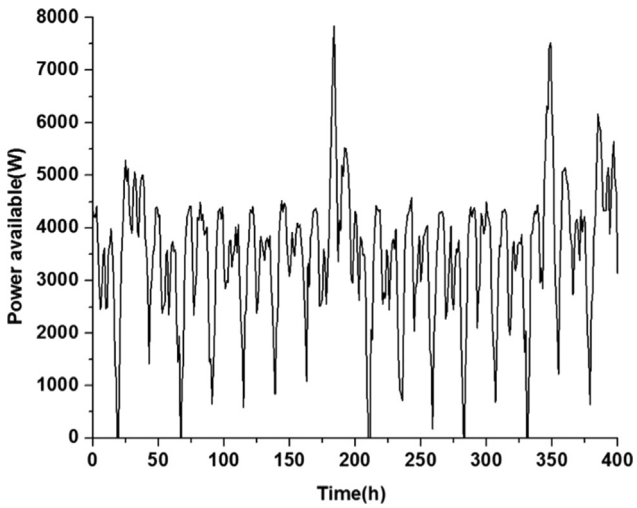

Fig. 14. $P_{\text{available}}$ to be absorbed.

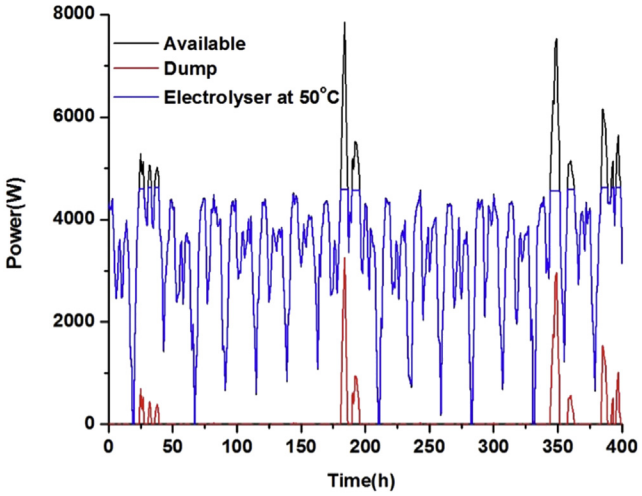

Fig. 15. P_{ele} and P_{dump}.

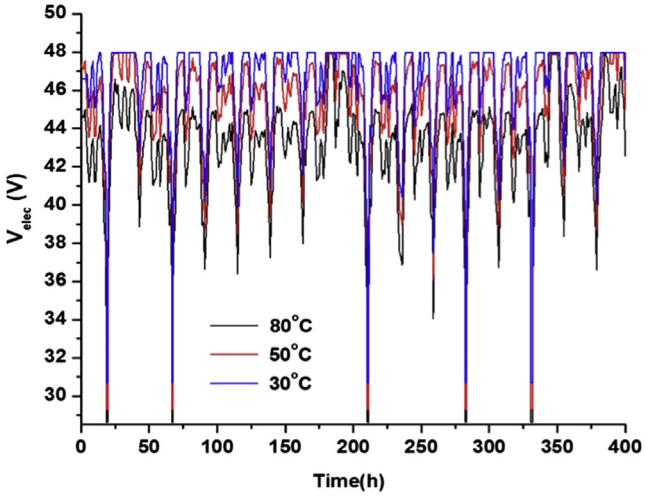

Fig. 16. V_{ele} at different temperatures.

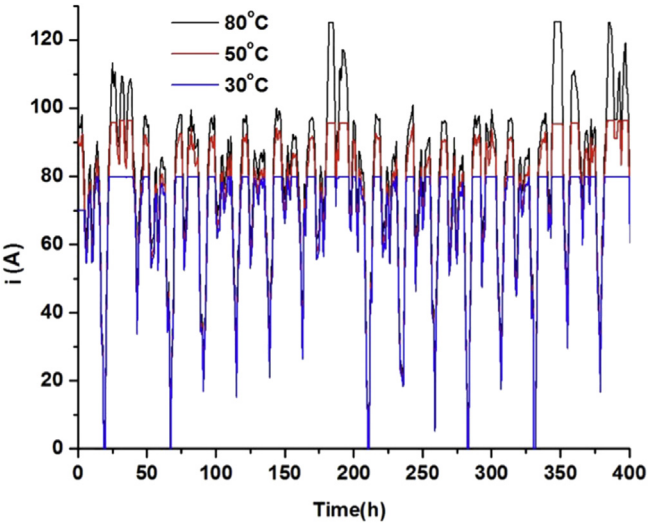

Fig. 17. Electrolyser's operating current at different temperatures.

$$\alpha = 0.94\frac{P_{available}}{P_{ele}} + 0.003(P_{available} - P_{ele}) \quad (36)$$

Case 3. : If $P_{available} > P_{ele\text{-}max}$, the electrolyser is turned on and the duty cycle of the buck converter is set to its maximum. In this case, the dump load is activated and its power is computed by using (34) in order to keep a power balance.

The electrolyser temperature has been set to 50 °C. The power absorbed by the electrolyser and the dump load are plotted in Fig. 15. Clearly $P_{available}$ is absorbed mostly by the electrolyser, and the dump load comes in to play only infrequently. $P_{ele\text{-}max}$ for operating at 50 °C is equal to 4627 W. The variations of the electrolyser voltage and current, for three different operating temperatures, are plotted in Figs. 16 and 17.

5. Conclusions

A model for alkaline electrolysers has been developed considering a physics-based approach. This approach takes into account all quantifiable physical descriptors of the various phenomena appearing on the electrodes or the membrane or in the electrolyte-contact resistances, threshold voltages, bubble formation, etc. The operating temperature, pressure, electrolyte concentration and current have been defined as the inputs of the electrolyser model. This proposed physics model is able to replicate the i–V characteristic curve as well as the electrolyser's performance.

An electrical analogy of the electrolyser consisting of series arrangement of resistances and diodes has also been developed, each of these components reflecting the various physical effects taking place inside the electrolyser. The electrolyser's electrical analogy coupled with the physics model have been integrated into an electrical simulations system called an Alkaline Electrolyser Simulation Tool (AEST). The integration of the given power electronics devices and AEST using the Hydrogen Research Institute electrolyser configuration is explained in this paper, as well as the i–V characteristics resulting from the simulation. Comparison with experimental values is excellent. Using this new approach the current i becomes a reaction of the process (imposing a V on the electrolyser), therefore the imposed V acts as an input in the AEST.

Finally the proposed AEST has been used to emulate the physical dynamics of a hybrid electrical system consisting of a diesel generator, a load network, and the electrolyser used to produce hydrogen during those phases of the system when excess power is available. The AEST is able to predict hydrogen production using the simulated operating electrolyser's current, to emulate the impact of the electrolyser in power electronics and the impact of electrical sources, power electronics, temperature, pressure, electrolyte concentration on the physical and electrical response of the electrolyser.

AEST is a useful tool for predicting and emulating the alkaline electrolyser's performance and the hydrogen production in long-term (steady-state) scenarios as well. It could be used as an excellent tool to evaluate control strategies in systems with wind energy influences. The number of required parameters used in the model permits the characterization of any alkaline electrolyser.

Acknowledgments

This work was supported in part by the LTE of Hydro-Québec, H2CAN Network, Natural Resources Canada, the Natural Sciences and Engineering Research Council of Canada and the Bureau de

l'efficacité et de l'innovation énergétiques, Ministère des Ressources naturelles et de la Faune du Québec.

References

[1] J.P. Vanhanen, P.D. Lund, Int. J. Hydrogen 20 (7) (1995) 575–585.
[2] Ø. Ulleberg, Int. J. Hydrogen 28 (1) (2003) 21–33.
[3] S. Kelouwani, K. Agbossou, R. Chahine, J. Power Sources 140 (2) (2005) 392–399.
[4] G. Schiller, R. Henne, P. Mohr, V. Peinecke, Int. J. Hydrogen 23 (9) (1998) 761–765.
[5] K. Zeng, D. Zhang, Prog. Energy Combust. Sci. 36 (3) (2010) 307–326.
[6] K.S. Agbli, M.C. Péra, D. Hissel, O. Rallières, C. Turpin, I. Doumbia, Int. J. Hydrogen 36 (2) (2011) 1382–1398.
[7] M. Hammoudi, C. Henao, K. Agbossou, Y. Dubé, M.L. Doumbia, Int. J. Hydrogen 37 (19) (2012) 13895–13913.
[8] J.G. Garcia Clua, H. De Battista, R.J. Mantz, Int. J. Hydrogen 35 (11) (2010) 5786–5792.
[9] A. Garrigos, J.M. Blanes, J.A. Carrasco, J.L. Lizan, R. Beneito, J.A. Molina, Int. J. Hydrogen 35 (12) (2010) 6123–6130.
[10] R. Takahashi, H. Kinoshita, T. Murata, J. Tamura, M. Sugimasa, A. Komura, M. Futami, M. Ichinose, K. Ide, IEEE Trans. Ind. Electron. 57 (2) (2010) 485–493.
[11] O. Atlam, M. Kolhe, Energy Convers. Manag. 52 (8–9) (2011) 2952–2957.
[12] T. Senjyu, T. Nakaji, K. Uezato, T. Funabashi, IEEE Trans. Energy Convers. 20 (2) (2005) 406–414.
[13] D.J. Lee, L. Wang, IEEE Trans. Energy Convers. 23 (1) (2008) 311–320.
[14] R.L. LeRoy, C.T. Bowen, D.J. LeRoy, J. Electrochem. Soc. 127 (9) (1980) 1954–1962.
[15] J. Eigeldinger, H. Vogt, Electrochim. Acta 45 (27) (2000) 4449–4456.
[16] H. Vogt, R.J. Balzer, Electrochim. Acta 50 (10) (2005) 2073–2079.
[17] M.F. Kibria, M.Sh. Mridha, A.H. Khan, Int. J. Hydrogen 20 (6) (1995) 435–440.
[18] M.F. Kibria, M.Sh. Mridha, A.H. Khan, Int. J. Hydrogen 21 (3) (1996) 179–182.
[19] J.Y. Huot, J. Electrochem. Soc. 136 (7) (1989) 1933–1939.
[20] M.H. Miles, G. Kissel, P.W.T. Lu, S. Srinivasan, J. Electrochem. Soc. 123 (3) (1976) 332–336.
[21] R.J. Gilliam, J.W. Graydon, D.W. Kirk, S.J. Thorpe, Int. J. Hydrogen 32 (3) (2007) 359–364.
[22] D.M. See, R.E. White, J. Chem. Eng. Data 42 (6) (1997) 1266–1268.
[23] M.P.M.G. Weijs, L.J.J. Janssen, G.J. Visser, J. Appl. Electrochem. 27 (4) (1997) 371–378.
[24] H. Vogt, J. Appl. Electrochem. 13 (1983) 87–88.
[25] Ph. Vermeiren, W. Adriansens, J.P. Moreels, R. Leysen, Int. J. Hydrogen 23 (5) (1998) 321–324.
[26] K. Agbossou, M.L. Doumbia, A. Anouar, Ind. Appl. Conf. 4 (2–6) (2005) 2932–2936.
[27] E. Troncoso, M. Newborough, Int. J. Hydrogen 36 (1) (2011) 120–134.
[28] R.J. Mantz, H. De Battista, Int. J. Hydrogen 33 (16) (2008) 4291–4300.
[29] M. Korpas, C.J. Greiner, Renew. Energy 33 (6) (2008) 1199–1208.
[30] C. Koroneos, E. Katopodi, Renew. Sustain. Energy Rev. 15 (1) (2011) 648–656.